






Pan-Atlantic decadal climate oscillation linked to ocean circulation

Hyacinth C. Nnamchi^{1,2}, Riccardo Farneti³, Noel S. Keenlyside⁴, Fred Kucharski³, Mojib Latif^{1,5}, Annika Reintges⁶ & Thomas Martin¹

Atlantic climate displays an oscillatory mode at a period of 10–15 years described as pan-Atlantic decadal oscillation. Prevailing theories on the mode are based on thermodynamic air-sea interactions and the role of ocean circulation remains uncertain. Here we uncover ocean circulation variability associated with the pan-Atlantic decadal oscillation using observational datasets from 1900–2009. Specifically, a sea level-derived index of ocean circulation also exhibits 10–15 year periodicity and leads the surface climate oscillation. The underlying ocean circulation links the extratropical and tropical Atlantic, where the maximum variance in surface-ocean temperature feeds back on the North Atlantic Oscillation (the leading mode of atmospheric variability over the North Atlantic region). Our findings imply that, rather than a passive role postulated by the thermodynamic paradigm, ocean circulation across the Atlantic plays an active role for the pan-Atlantic decadal climate oscillation.

¹GEOMAR Helmholtz Centre for Ocean Research Kiel, Düsternbrooker Weg20, 24105 Kiel, Germany. ²Department of Geography, University of Nigeria, Nsukka 410001, Nigeria. ³Earth System Physics Section, Abdus Salam International Centre for Theoretical Physics, Strada Costiera 11, 34151 Trieste, Italy. ⁴Geophysical Institute and Bjerknes Centre for Climate Research, University of Bergen, Allégaten 70, 5007 Bergen, Norway. ⁵Kiel University, Christian-Albrechts-Platz 4, 24118 Kiel, Germany. ⁶National Centre for Atmospheric Science, University of Reading, Reading, UK. ✉email: hnnamchi@geomar.de

The extreme climate conditions across the Northern Hemisphere during the 2009/10 winter season¹, and the subsequent active Atlantic hurricane season², have been suggested to be part of an anomalous climate state in the Atlantic Ocean. For example, a tripole-anomaly structure characterized the sea surface temperature (SST) in the North Atlantic: warm in the main hurricane development region of the tropical North Atlantic³, cold in the subtropics, and warm in the subpolar North Atlantic⁴. The midlatitude westerlies weakened and temporarily reversed direction¹. These conditions were associated with a severe negative phase of the North Atlantic Oscillation (NAO), and extreme cold surface air temperatures across western Europe^{1,4}, warm surface temperatures and summer heatwaves over western Russia^{5,6}. The increased upper-ocean temperatures in the tropical North Atlantic favoured the accumulation of energy accessible to hurricanes², a re-emergence of the tripole pattern⁴ and an extreme negative NAO during the 2010/2011 winter^{5,7}. The year 2010 was exceptionally warm and wet over West Africa, the rainy season being the wettest since 1958 in the semi-arid Sahel⁸.

Observations of the Atlantic Meridional Overturning Circulation (AMOC) at 26.5°N—the system of northward-flowing warm, upper-ocean currents and southward-flowing deep, dense waters—featured a substantial slowdown in 2009/10^{2,8}. In the following years, this was accompanied by a swing to the positive NAO phase⁹, reduced northward ocean heat transport¹⁰, decreased heat content¹¹, and increased freshening¹² in the subpolar North Atlantic. The changes in the Atlantic sector climate system peaked in 2015^{9,12} and were linked to the pervasive European heatwaves during the summer of that year¹³. Indeed, the characteristic north-south bands of SST anomalies observed in the Atlantic in 2009/10⁷ have previously been linked to variations in Atlantic hurricanes¹⁴, global surface-air temperature¹⁵, Sahel rainfall¹⁶, South American, North American and European climates^{17,18}.

By analyzing observational datasets from 1900–2009, we find that the occurrence of these patterns, which in 2009/2010 coincided with a prevailing positive phase of the Atlantic Multidecadal Oscillation¹⁹, constitute a 10–15 year pan-Atlantic decadal oscillation (ADO) linked to ocean circulation. A sea level-derived index of ocean circulation variability^{20–22} leads the ADO pattern by 2 years, through the interactions of AMOC and gyre circulations with Kelvin wave anomalies that propagate from the North Atlantic to the low latitudes and by thermocline feedback in the Atlantic cold tongue region. The mature phase of the ADO exhibits maximum SST variance in the tropical Atlantic which, in turn, drives inter-hemispheric atmospheric teleconnections represented by negative NAO phase over the North Atlantic. We conclude that, rather than a passive role postulated by the prevailing thermodynamic paradigm^{17,23}, ocean circulation plays an active role for ADO variability.

Results

Sea level-derived ocean-circulation index. Direct AMOC measurements from the RAPID-MOCHA monitoring array along 26.5°N are only available since 2004²⁴. Nonetheless, proxies of AMOC variability during the twentieth century can be reconstructed using observations of other variables. In particular, dynamic sea level—the deviation from the globally averaged sea level—captures variations of the ocean depth-integrated density²⁵. The large-scale ocean circulation is essentially geostrophic in the North Atlantic, and increased (decreased) overturning transport is associated with a decline (rise) in sea level along the western boundary north of Cape Hatteras^{20–22}. As a result, sea-level variability along the northeast coast of North America, north of Cape Hatteras, where multiple measurement

sites date back to the early twentieth century²², is considered as a proxy of the AMOC variability^{20–22}.

We construct a composite sea-level index of ocean circulation by averaging records from 24 tide gauge sites along the northeast coast of the United States from Portsmouth to Boston (Supplementary Fig. 1). The sea-level index has been deseasonalised, linearly detrended and inverted so that positive (negative) values corresponds to increased (reduced) overturning transport. The monthly index displays strong variability from 1900 to 2009 with a standard deviation of 56 mm. We investigate ocean-circulation variability by normalizing the sea-level index by its standard deviation (Fig. 1a).

Our sea level-derived index of ocean circulation is correlated with the monthly RAPID-MOCHA-derived AMOC data during the observational period 2005–2019 ($r = 0.50$; $p = 1.48 \times 10^{-9}$). The AMOC at 26.5°N exhibits a marked seasonality²⁵ with strongest variability in boreal winter associated with geostrophic transport²⁵ and North Atlantic Deep Water variability, that reflect wintertime atmospheric variability over the North Atlantic region^{26–28}. Similarly, the AMOC correlation with the sea-level index peaks in winter ($r = 0.72$; see Supplementary Table 1 and Fig. 1c). This is statistically significant at the 99.9% confidence level after accounting for autocorrelation in both time series (see Methods). We also accounted for uncertainty in this analysis by repeating the calculations using different sections of the time series, with overall strong correlation ($r = 0.77 \pm 0.04$, $p = 0.0023 \pm 0.0021$). This represents 53–66% explained variance, which supports the hypothesis that sea level along the east coast of United States responds to overturning variability^{20–22}. Indeed, the sea level-derived index of ocean circulation closely captures the evolution of the RAPID-MOCHA observations from 2005 to 2019, including the widely discussed 2009/2010 slowing event but with smaller amplitude (Fig. 1c). Because our sea level-derived index is influenced by multiple factors including gyre and overturning ocean circulations^{21,22}, we consider the sea level-derived index to describe variability in the ocean-circulation generally.

Spectral analysis of the sea-level index yields a dominant peak at a period of 147 months (Fig. 1b), which suggests a 12.3 year variability in ocean circulation and is also seen in the December–February data (Fig. 1d). In addition, the monthly spectrum displays some robust high (<10 years) and low-frequency (>15 years) peaks. These represent interannual and multidecadal ocean-circulation variability discussed elsewhere using high-pass²⁰ and low-pass²⁹ filtered versions of similar sea level-derived indices. Our sea level-based index of ocean circulation variability is correlated with the sea level difference between the subtropical and subpolar gyres²¹ only in certain epochs (Supplementary Fig. 2a) such as 1950–1970 ($r = 0.61$; $p = 0.0031$) and 1990–2009 ($r = 0.71$; $p = 0.0005$). However, the 12.3 year periodicity is somewhat muted in the sea level-difference index (Supplementary Fig. 2b) that may better represent multidecadal variability²¹.

The present study is focused on variability at the dominant 12.3-year period in our index. The spectral variance, however, is distributed in a band of about 10 to 15 years (shown by the vertical grey bar in Fig. 1b, d). This is insensitive to using different time slices of the monthly time series which better resolves the 10–15 year peak (Fig. 1b) compared to the seasonally-averaged data (Fig. 1d). Here we analyse the annual patterns associated with the 10–15 year variability 1900–2009. Questions such as seasonality and stationarity of the patterns including the possible impacts of decadal shift around 1987 in the North Atlantic^{30,31} need to be investigated in further studies.

Mode of variability. Similar to our ocean-circulation index, patterns of air–sea interaction with periodicity of 10–15 years

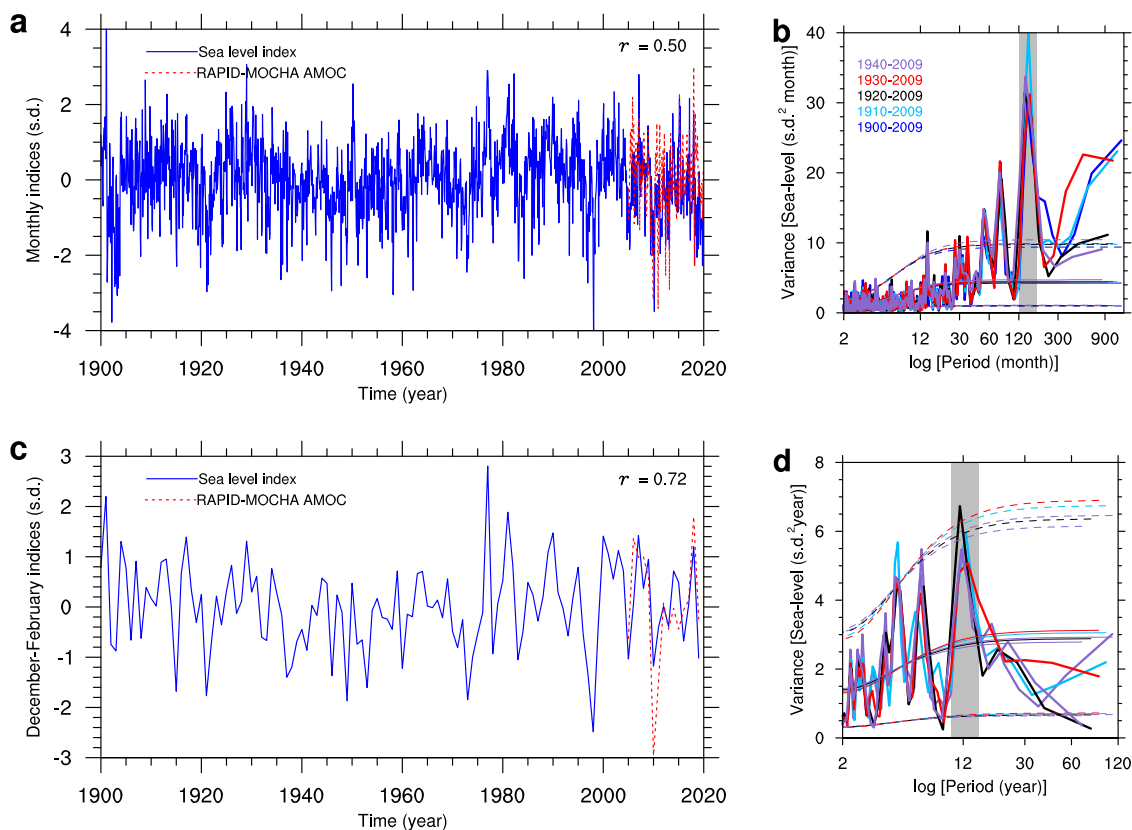


Fig. 1 The sea level-derived ocean circulation index. **a** Normalized monthly sea-level index used as a proxy for ocean circulation variability (solid, blue curve) 1900–2019 and AMOC measurements from the RAPID-MOCHA array (dashed, red curve, 2005–2019). **b** Spectra of the monthly sea-level index (thick, solid), its first-order autoregressive fit (solid, thin) and 95% confidence bounds (thin, dashed) for the different time slices indicated in the top-left corner of **(b)**. **c**, **d** Similar to **(a)**, **(b)**, respectively, but based on December–February data. The correlations (r) between the sea-level and AMOC time series for the common period from 2005 to 2019 are indicated in the top-right corner of **(a)**, **(c)**. The vertical grey bars in **(b)**, **(d)** show the 10–15 year period band.

have been observed in different parts of the Atlantic. Examples are the tripole pattern of SST in the North Atlantic linked to the NAO³², a cross-equatorial SST gradient in tropical Atlantic associated with changes in trade winds in both hemispheres³³, and a dipole structure in the South Atlantic linked to the southeasterly trade winds and subtropical anticyclone³⁴. Indeed, using composite analysis, it has been suggested²³ that these patterns constitute regional expressions of a pan-Atlantic pattern, the ADO.

We perform an Empirical Orthogonal Function (EOF) analysis of the Atlantic monthly SST anomalies during 1900–2009. The second mode (EOF2) accounting for approximately 11% of the variance is the ADO (Fig. 2a). The first mode accounts for about 15% of the variance and represents the Atlantic Multidecadal Oscillation (Supplementary Fig. 3). The spectrum of the principal component of EOF2 (PC2) exhibits a major peak at the 10–15 year periodicity (Fig. 2b, c), suggesting a close link of the ADO to the Atlantic ocean-circulation variability. The 10–15 year peak is clearly very dominant in the unfiltered time series. As a result, we do not apply any form of low-pass³⁵ or band-pass³⁶ filters, commonly used in decadal climate studies but can induce spurious low-frequency signals³⁵.

The ADO, as defined by EOF2, exhibits meridional bands of alternate SST anomalies from the extratropical South Atlantic all the way to Greenland (Fig. 2a). The largest local explained variance is found in the tropical Atlantic³⁷. The associated wind-stress anomalies are indicative of weaker midlatitude westerlies over the North Atlantic³², stronger (weaker) southeasterly (northeasterly) trade winds to the south (north) of the equator, and cross-equatorial flow^{17,23,33}. The SST and wind-stress

anomalies over the tropical North Atlantic can be linked to a northerly displacement of the Inter-Tropical Convergence Zone (ITCZ)^{17,33}. An index of the ITCZ is closely related to an ADO-type cross-equatorial anomalies in vertical gradient of diabatic heating (Supplementary 4a, b), which determines the atmosphere’s sensitivity to SST anomalies in the tropical Atlantic³⁸. The ITCZ index also displays a prominent 10–15 year periodicity, and is highly coherent with SST PC2 (above the 95% confidence level; Supplementary Fig. 4c, d). However, there is no phase lag in the 10–15 year band, suggesting that the ITCZ and SST variability mutually reinforce each other.

The role of ocean circulation. Given the common 10–15 year periodicity of SST PC2 and the sea level-derived ocean circulation index, we hypothesize that the ADO is driven by variability in ocean circulation. The related variability in sea surface height, a proxy for ocean circulation and upper-ocean heat content variability³⁹, exhibits a meridional structure that is similar to the SST pattern regressed on SST PC2 (Fig. 3a). Generally speaking, regions of warm (cold) SST anomalies in the Atlantic correspond to increased (decreased) heat content and consequently rise (decline) in sea surface height anomalies (Figs. 2a, 3a).

We further investigate the role of ocean circulation using cross-spectral analysis. Our sea-level derived index of ocean circulation is highly coherent (above the 95% confidence level) with both SST PC2 and ITCZ in the 10–15 year band (Fig. 3b, c). The phase lags are remarkably similar and close to $\pi/3$ radians (or 2 years), with the sea level-based ocean circulation index leading. Thus, this analysis supports our hypothesis that the SST variability is driven

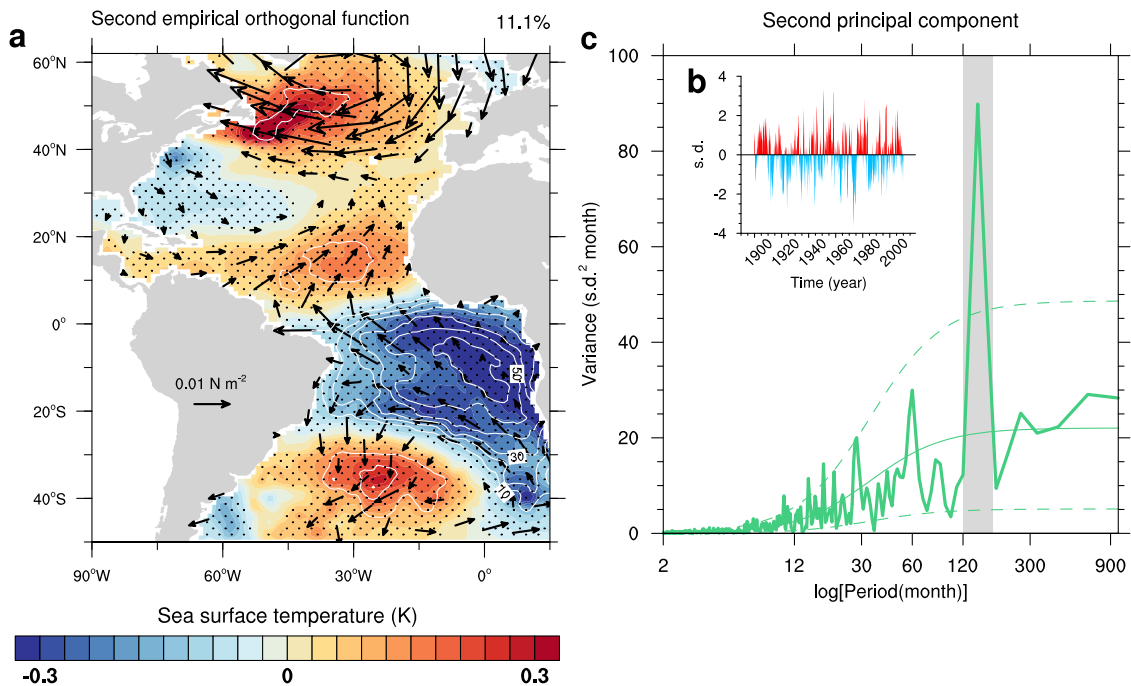


Fig. 2 EOF2 of monthly SST anomalies in the Atlantic. **a** SST (color-scale) and wind stress anomalies (arrows, only statistically significant vectors are shown) regressed onto the normalized SST PC2 time series. The stippling in **(a)** denotes statistical significance at 95% confidence level. **b** Time evolution of the SST PC2 and **(c)** its spectrum (thick, solid curve); the associated first-order autoregressive spectrum (thin, solid curve) and the 95% confidence bounds (thin, dashed curves). The grey vertical bar shows the 10–15 years periodicity band.

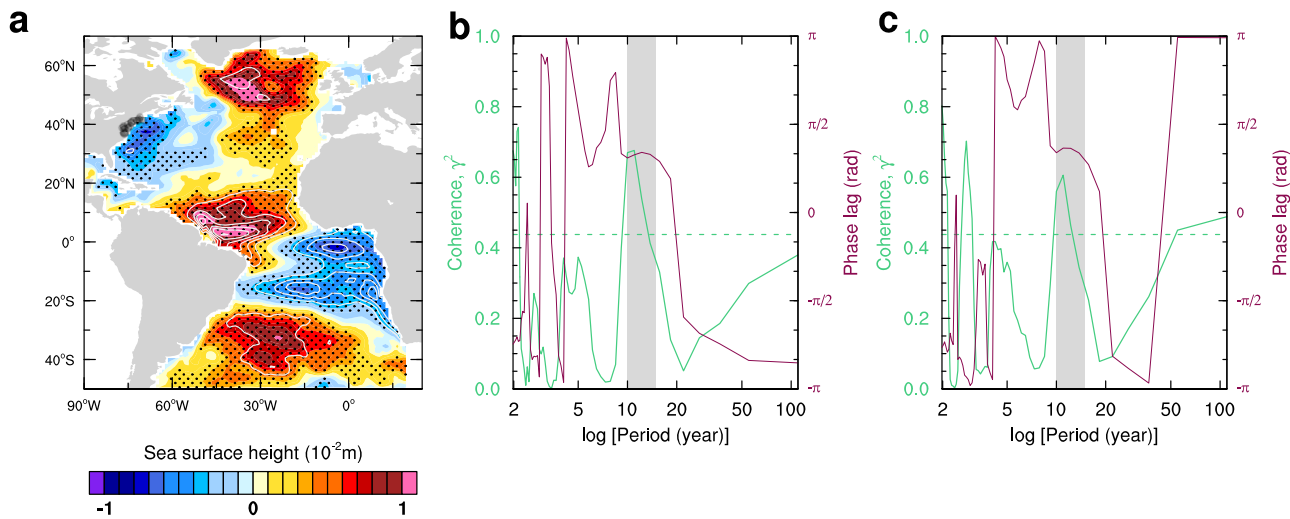


Fig. 3 Relating SST PC2 to sea surface height and sea-level index. **a** Monthly anomalies of sea surface height regressed onto the normalized SST PC2 time series. Stippling denotes statistical significance at 95% confidence level; white contours denote explained variances at interval of 3%. The tide-gauge sites used along the United States northeast coast 37–42°N are marked black. **b, c** Coherence (left axis) and phase lag (right axis) between sea-level index and **b** SST PC2 and **c** ITCZ. The sea-level index leads (follows) PC2/ITCZ at positive (negative) lags. The vertical grey bar shows the 10–15 year period band. The dashed horizontal line denotes 95% confidence level for squared coherence.

by ocean circulation. This interpretation does not change when using the post-World War II period, with pattern correlations greater than 0.80 between the 1900–2009 and 1950–2009 periods for the maps analyzed (Supplementary Table 2).

Previous studies suggest that the 10–15 year timescale originates from variability in air–sea interactions, thermohaline circulation, and Arctic sea-ice outflow in high-latitude North Atlantic^{23,40}. Here we analyse reconstructed turbulent surface fluxes⁴¹ averaged over the North Atlantic region (40–50°N, 20–60°W) to show a 10–15 year coherence with the sea level

index in winter when the ocean circulation variability is particularly strong^{25–28} (Supplementary Fig. 5). The turbulent fluxes lead the 10–15 year peak in the December–February sea level-based index of ocean circulation (Fig. 1d; Supplementary Fig. 5).

In models of ocean circulation, atmospheric forcing in high-latitude North Atlantic excites AMOC variations along the western boundary^{42,43}, part of which is advected into the interior ocean near Flemish Cap and the Grand Banks⁴⁴. In the subtropics, the southward-flow is confined to the western

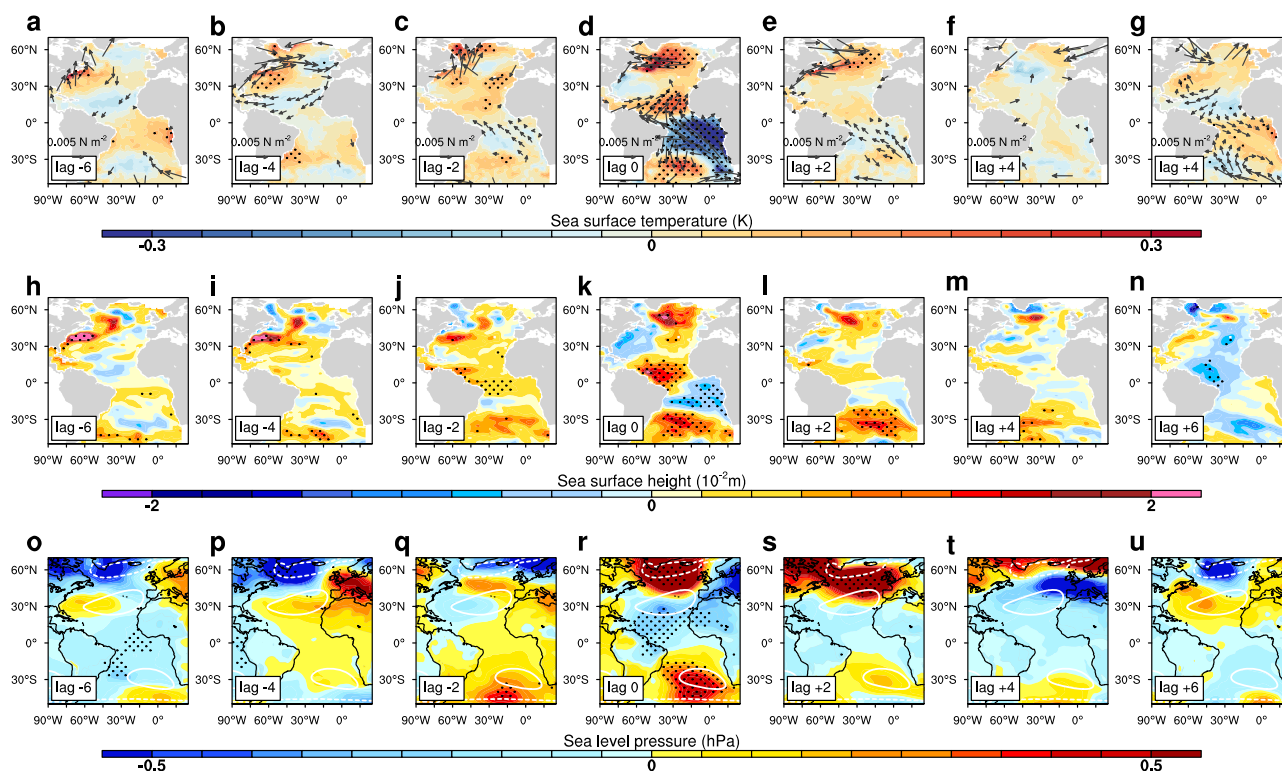


Fig. 4 Evolution of the related air-sea interactions. **a–g** Anomalies of the SST (colour-scale) and wind stress (arrows, only statistically significant vectors are shown), **(h–n)** sea surface height and **(o–u)** sea level pressure lag-regressed on the SST PC2. In all panels, stipples denote statistical significance at 95% confidence level. In **(o–u)**, the white contours show regions of mean annual high pressure (1018 hPa, solid) and low pressure (1008 hPa, dashed). Panels **(a–n)** **(o–u)** are based on annual (December–February) data.

boundary as coastal Kelvin waves^{42–44}. The Kelvin waves are deflected across the basin at the equator, which acts as a low-pass filter, and then propagate poleward along the eastern boundary of both hemispheres⁴⁵. Thus, ADO-related heat content anomalies in North Atlantic lead the anomalies in the tropical Atlantic as suggested by the sea surface height analysis (Fig. 4h–n). The delay of the flow along the interior pathways⁴⁴ may explain the 2-year lag between our sea-level index (constructed using tide-gauges in the region 37–42°N) and SST PC2. This is consistent with a 5-year lag between observational Labrador Sea Water thickness and tropical Atlantic SST variability⁴².

Thermodynamic air–sea interactions represented by the wind–evaporation–SST mechanism may amplify the ADO-related patterns through turbulent surface–heat fluxes^{17,23,32,33}. This mechanism operates even under motionless ocean conditions in simplified climate models^{23,33}, and is associated with variability of the subtropical anticyclones and meridional displacements of the ITCZ³³. Turbulent fluxes drive phase change in ocean circulation⁴¹ (Supplementary Fig. 5) and northward heat transport from the subtropical gyre towards the subpolar gyre of North Atlantic²¹. About 70% of the northward-flowing water masses loop through the subtropical gyre—at a period of 14 years in the upper-ocean in an eddy-permitting (1/4° resolution) Earth system model—to become sufficiently dense, and then continue northwards⁴⁵. The period is 22 years in a coarse (1° resolution) version of the model⁴⁵, consistent with 20–30 year periodicity of AMOC-type response to atmospheric forcing in coarse resolution ocean models^{46,47}. These findings point to the interaction of the AMOC and gyre circulations with Kelvin waves in setting the 10–15 periodicity.

The northward shift of the ITCZ is linked to a strengthening (weakening) of the southeast (northeast) trade winds in the Southern (Northern) Hemisphere⁴⁸ (Fig. 4a–g), and development

of a negative NAO pattern over the North Atlantic (Fig. 4a–g, o–u). The stronger-than-normal southeasterly trades (Fig. 4) drive increased upwelling to the east in the Atlantic cold tongue region (as suggested by Fig. 3a, Fig. 4k). This implies shallower (deeper)-than-normal thermocline in the east (west) and increased east-west thermocline slope.

The east-west thermocline gradient index (ΔH), as a measure of ocean circulation variability in the cold tongue, displays interannual to decadal fluctuations with multidecadal shifts particularly during the first half of the twentieth century (Fig. 5a). The ΔH is correlated with the SST PC2 using monthly ($r = 0.38$, $p = 2.95 \times 10^{-14}$) and annual ($r = 0.45$, $p = 7.79 \times 10^{-7}$) time series. Furthermore, the ΔH spectrum also exhibits a peak at the 10–15 year periodicity of interest (Fig. 5b). In addition to the well-known interannual timescales¹⁷, ΔH is significantly coherent with cold tongue SST variability represented by the Atlantic Niño index in the 10–15 year period band (Fig. 5c). The phase lag is close to π radians or 180°, indicating that large ΔH goes along with anomalously cold SST.

Discussion

We present observational evidence of a 10–15 year periodicity of ocean circulation in the Atlantic that leads ADO-type climate variability. Potentially forced from the North Atlantic^{23,40}, the ADO-related changes propagate to the tropical and South Atlantic through alterations in oceanic and atmospheric circulations^{23,40,43–45}. Maximum variance of the 10–15 year pattern is associated with strong thermocline feedback in the Atlantic cold tongue region, which drives SST anomalies and atmospheric teleconnections in both hemispheres²³, giving rise to negative NAO phase in winter over the North Atlantic^{49,50}. The wintertime atmospheric variability is related to strong geostrophic

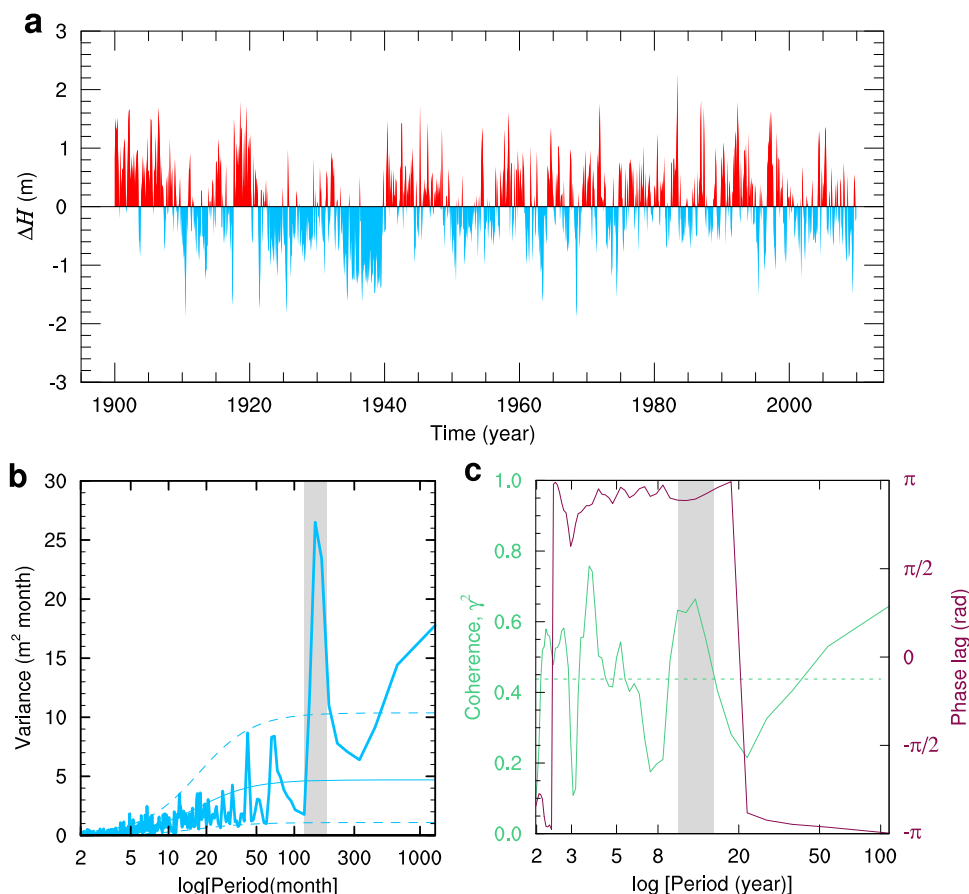


Fig. 5 Analysis of cold tongue dynamics. **a** Monthly ΔH time series and **(b)** spectrum (thick, solid curve); associated first-order autoregressive curve (thin, solid curve) and the 95% confidence bounds (thin, dashed curves). **c** Coherence (left axis) and phase lag (right axis) between annual ΔH and Atlantic Niño index. The dashed horizontal line denotes 95% confidence level for spectral coherence. The ΔH leads at positive lags whereas Atlantic Niño leads at negative lags. The vertical bar in both panels shows the 10–15 year period band.

transport²⁵ and North Atlantic Deep Water variability^{26–28}. Diabatic heating associated with the Atlantic ITCZ is linked to the circulation over the North Atlantic sector⁵¹, and modelling studies indicate tropical Atlantic SST similar to those described here can induce a NAO like response⁵². The NAO also exhibits strong variability in the decadal band^{53–55}.

The leading role of ocean circulation we discuss may explain the relatively small variances explained by heat fluxes over the North Atlantic region (10–45°N, 20–60°W) in an observational analysis of the 2009/10 extreme event⁵⁶. Our results close a key knowledge-gap by linking the impacts of ocean circulation on the climate variability across the entire Atlantic basin. These findings imply that the ADO pattern is potentially more predictable than previously thought, and possibly underlies the skillful decadal predictions of surface-climate variability over the North Atlantic sector in an ensemble of climate model simulations^{57,58}.

Methods

Data. We constructed a sea level-based index of ocean circulation by averaging observations of monthly sea level (unit, mm) from 24 tide gauge sites on the US northeast coast, north of Cape Hatteras from Portsmouth to Boston, representing the “Northern Sites” discussed in McCarthy et al.²¹ (Supplementary Fig. 1). The sea-level observations across this region exhibits a spatially-coherent variability that has been closely linked to the AMOC variability^{20–22,29}. We also analyzed observations of SST on $1^\circ \times 1^\circ$ global longitude–latitude grids⁵⁹ and the European Centre for Medium-Range Weather Forecasts twentieth century ocean reanalysis of sea surface height, a proxy for the upper-ocean heat content, on $1^\circ \times 1^\circ$ longitude–latitude with equatorial refinement of 0.3° and 42 vertical levels⁶⁰. In addition, wind stress, sea level pressure, wind components, specific humidity, air

temperature, air pressure and vertical velocity were taken from the twentieth century atmospheric reanalysis⁶¹ on $1.25^\circ \times 1.25^\circ$ and 37 pressure levels.

We analysed the sea level-derived index of ocean-circulation, atmospheric and oceanic fields for the common period 1900–2009, with the patterns strongly correlated with those of 1950–2009 period (Supplementary Table 2). This is consistent with previous studies that show similar 10–15 year meridional patterns of SST variability in the North Atlantic⁴⁰ (1948–2017), tropical Atlantic³³ (1950–1989), and South Atlantic³⁴ (1953–1992) using post-World War II observations. For comparison with the RAPID-MOCHA AMOC (2005–2019), the sea-level index is extended to 2019 in Fig. 1a, c and Supplementary Table 1.

For all variables, we estimated and subtracted the least-squares linear trends from the data prior to subsequent analysis. This removes the effects of external climate forcing such as anthropogenic greenhouse effect and also any possible land subsidence effects in case of the sea level time series, and thus allows us to focus on intrinsic variability of the Atlantic climate.

Diabatic heating. We estimated the diabatic heating rate (Q_1) as a residual of the atmospheric heat budget⁶²:

$$Q_1 = \frac{\partial T}{\partial t} - \left(\omega \sigma - \frac{u \partial T}{\partial x} + \frac{v \partial T}{\partial y} \right) \quad (1)$$

where T denotes the air temperature, u the zonal wind component, v the meridional wind component, ω the vertical pressure velocity, σ the static stability given by:

$$\sigma = \frac{RT}{C_p p} - \frac{\partial T}{\partial p} \quad (2)$$

R is the gas constant ($R = 287 \text{ J kg}^{-1} \text{ K}^{-1}$), p the air pressure and C_p the specific heat capacity at constant pressure ($C_p = 1004.64 \text{ J kg}^{-1} \text{ K}^{-1}$). Differential operators, x , y and t , are along zonal and meridional directions, and time, respectively. Q_1 was first computed for all atmospheric levels using daily data and then averaged to monthly data. The vertical gradient was determined by

subtracting the values at the surface (1000 hPa) from the values in the mid-troposphere (400 hPa), that is, mid-troposphere *minus* the surface.

ITCZ, ΔH and Atlantic Niño indices. We estimated the ITCZ location as the linearly interpolated latitude at which the meridional wind stress equals zero over the tropical Atlantic region 5°S–20°N. The estimated latitudes were then averaged between 30°W and 40°W to create a simple composite index time series. A larger (smaller) value of this index implies a more (less) northerly position of the ITCZ.

ΔH is a measure of the thermocline slope in the equatorial Atlantic cold tongue region, given by east-west gradient of the thermocline in that region. We first estimate the depth of 20°C isotherm and then average in the cold tongue region (3°N–3°S) as a proxy for the equatorial thermocline (H), and the gradient (ΔH) determined as:

$$\Delta H = H_{(20-40^\circ W)} - H_{(0-20^\circ W)} \quad (3)$$

where the subscripts represent the western (20–40°W) and eastern (0–20°W) regions of the basin, the overbar represents domain-averages. Using anomalies of H , positive ΔH represents increased slope and negative ΔH represents reduced slope. This measure is anti-correlated with cold tongue SST anomalies, so that stronger gradient is linked to negative SST anomalies in the eastern equatorial Atlantic.

The Atlantic Niño index is defined as the SST anomalies averaged over the eastern equatorial Atlantic Ocean region 3°N–3°S, 0–20°W.

EOF, correlation and regression analysis. We performed EOF analysis to identify the ADO as the second mode, whereas the first mode denotes the AMO pattern in the Atlantic Ocean. The EOF analysis was based monthly SST anomalies from 1900 to 2009 over the Atlantic Ocean using basin mask from the World Ocean Circulation Experiment. The two leading modes account for about 26% of the total variance, and are separated from each other according to a simple eigenvalue separation principle⁶³.

We use Pearson's r and least-squares estimates for the correlation and regression analysis, respectively. Both estimates were tested for statistical significance using two-tailed Student t -test and the 95% confidence level marked. To account for autocorrelation, we adjusted the degrees of freedom of the time series pairs as follows⁶⁴:

$$N^* = N \frac{(1 - r_1 r_2)}{(1 + r_1 r_2)} \quad (4)$$

where N^* is the adjusted number of degrees of freedom used for computing the statistical significance, N is the length of the original time series, r_1 and r_2 are the lag-1 autocorrelation coefficients of the time series pairs, respectively.

Relating sea level and AMOC variability. The AMOC at 26.5°N exhibits a strong seasonality that is linked to geostrophic related transport²⁵. The strongest variability in the RAPID-MOCHA AMOC index occur in boreal winter when we also see strong variability in the sea-level index (Supplementary Table 1). Thus, the correlation between our sea level-based ocean circulation index and RAPID-MOCHA AMOC data 2005–2019 is seasonally-dependent, being strongest in December–February ($r = 0.72$). We accounted for uncertainty in the correlation using 12 time slices from 2005 to 2014–2019 and from 2005–2010 and 2019, and the associated p -values determined using the adjusted degrees of freedom. We then determined the uncertainty of the correlation coefficients, p -values and explained variances as the two standard deviations. The AMOC and sea-level indices are also significantly correlated in March–May.

However, the correlations are generally weak in other seasons and in annual data (Supplementary Table 1). This is consistent with poor correlations between AMOC and sea-level indices from the east coast of North America in some previous studies^{65,66}, whereas the sea level variability has also been linked to atmospheric influences⁶⁶.

Spectral and cross-spectral analysis. The spectral and cross-spectral analyses were performed by an autoregressive fitting of data based on the maximum entropy method⁶⁷. The spectrum was smoothed by a three-point Daniell filter⁶⁸, and compared with a theoretical red noise spectrum based on the first-order autoregressive model, with the upper and lower 95% confidence bounds marked. The 10–15 year oscillation is practically insensitive to the order of autoregressive model⁶⁹. The cross-spectrum was smoothed by a seven-point Daniell filter with the squared-coherence and associated 95% confidence level⁷⁰ shown.

Data availability

All data used in this study are publicly available. Tide gauge data: www.psmsl.org; sea surface temperature: https://www.metoffice.gov.uk/hadobs/hadisst/data/HadISST_sst.nc.gz; RAPID-MOCHA AMOC: <https://doi.org/10.5285/cc1e34b3-3385-662b-e053-6c86abc03444>; ocean reanalysis: <ftp://ftp-icdc.cen.uni-hamburg.de/ora20c>; atmospheric

reanalysis: <https://rda.ucar.edu/datasets/ds626.0/> and turbulent heat fluxes: <https://doi.org/10.1038/nature12268>.

Code availability

Codes for the data analysis and preparation of the figures are openly available at https://github.com/hnnamchi/ado_commsenv.

Received: 2 October 2022; Accepted: 27 March 2023;

Published online: 14 April 2023

References

- Wang, C., Liu, H. & Lee, S.-K. The record-breaking cold temperatures during the winter of 2009/2010 in the Northern Hemisphere. *Atmos. Sci. Lett.* **11**, 161–168 (2010).
- Srokosz, M. A. & Bryden, H. L. Observing the Atlantic Meridional Overturning Circulation yields a decade of inevitable surprises. *Science* **348**, 1255575 (2015).
- Kossin, J. P. Hurricane intensification along United States Coast suppressed during active Hurricane Periods. *Nature* **541**, 390–393 (2017).
- Taws, S. L., Marsh, R., Wells, N. C. & Hirschi, J. Re-emerging ocean temperature anomalies in late-2010 associated with a repeat negative NAO. *Geophys. Res. Lett.* <https://doi.org/10.1029/2011GL048978> (2011).
- Maidens, A. et al. The influence of surface forcings on prediction of the North Atlantic Oscillation regime of winter 2010/11. *Mon. Weather Rev.* **141**, 3801–3813 (2013).
- Barriopedro, D., Fischer, E. M., Luterbacher, J., Trigo, R. M. & García-Herrera, R. The Hot Summer of 2010: Redrawing the temperature record map of Europe. *Science* **332**, 220–224 (2011).
- Buchan, J., Hirschi, J. J.-M., Blaker, A. T. & Sinha, B. North Atlantic SST Anomalies and the Cold North European weather events of Winter 2009/10 and December 2010. *Mon. Weather Rev.* **142**, 922–932 (2014).
- Blunden, J., Arndt, D. S. & Baringer, M. O. State of the Climate in 2010. *Bull. Am. Meteorol. Soc.* **92**, S1–S236 (2011).
- Josey, S. A. et al. The recent atlantic cold anomaly: causes, consequences, and related phenomena. *Ann. Rev. Mar. Sci.* **10**, 475–501 (2018).
- Smeed, D. A. et al. The North Atlantic Ocean is in a state of reduced overturning. *Geophys. Res. Lett.* **45**, 1527–1533 (2018).
- Bryden, H. L. et al. Reduction in ocean heat transport at 26°N since 2008 cools the eastern subpolar gyre of the North Atlantic Ocean. *J. Clim.* **33**, 1677–1689 (2020).
- Holliday, N. P. et al. Ocean circulation causes the largest freshening event for 120 years in eastern subpolar North Atlantic. *Nat. Commun.* **11**, 585 (2020).
- Duchez, A. et al. Drivers of exceptionally cold North Atlantic Ocean temperatures and their link to the 2015 European heat wave. *Environ. Res. Lett.* **11**, (2016).
- Kossin, J. P. & Vimont, D. J. A more general framework for understanding atlantic hurricane variability and trends. *Bull. Am. Meteorol. Soc.* <https://doi.org/10.1175/BAMS-88-11-1767> (2007).
- Mann, M. E. & Park, J. Global-scale modes of surface temperature variability on interannual to century timescales. *J. Geophys. Res.* <https://doi.org/10.1029/94jd02396> (1994).
- MORON, V. Trend, decadal and interannual variability in annual rainfall of subequatorial and tropical North Africa (1900–1994). *Int. J. Climatol.* **17**, 785–805 (1997).
- Foltz, G. R. et al. The Tropical Atlantic observing system. *Front. Mar. Sci.* **6**, 206 (2019).
- Ionita, M., Lohmann, G., Rimbu, N., Chelcea, S. & Dima, M. Interannual to decadal summer drought variability over Europe and its relationship to global sea surface temperature. *Clim. Dyn.* **38**, 363–377 (2012).
- Farneti, R. Modelling interdecadal climate variability and the role of the ocean. *WIREs Clim. Chang.* **8**, e441 (2017).
- Bingham, R. J. & Hughes, C. W. Signature of the Atlantic meridional overturning circulation in sea level along the east coast of North America. *Geophys. Res. Lett.* **36**, (2009).
- McCarthy, G. D., Haigh, I. D., Hirschi, J. J.-M. J. M., Grist, J. P. & Smeed, D. A. Ocean impact on decadal Atlantic climate variability revealed by sea-level observations. *Nature* **521**, 508–510 (2015).
- Little, C. M. et al. The Relationship Between U.S. East Coast Sea Level and the Atlantic Meridional Overturning Circulation: A Review. *J. Geophys. Res. Ocean.* **124**, 6435–6458 (2019).
- Xie, S. P. & Tanimoto, Y. A pan-Atlantic decadal climate oscillation. *Geophys. Res. Lett.* <https://doi.org/10.1029/98GL01525> (1998).

24. Frajka-Williams, E. et al. Atlantic meridional overturning circulation: Observed transport and variability. *Front. Mar. Sci.* <https://doi.org/10.3389/fmars.2019.00260> (2019).
25. Kanzow, T. et al. Seasonal variability of the Atlantic meridional overturning circulation at 26.5°N. *J. Clim.* **23**, 5678–5698 (2010).
26. Petit, T., Lozier, M. S., Josey, S. A. & Cunningham, S. A. Role of air–sea fluxes and ocean surface density in the production of deep waters in the eastern subpolar gyre of the North Atlantic. *Ocean Sci.* **17**, 1353–1365 (2021).
27. Megann, A., Blaker, A., Josey, S., New, A. & Sinha, B. Mechanisms for Late 20th and Early 21st Century Decadal AMOC Variability. *J. Geophys. Res. Ocean.* **126**, e2021JC017865 (2021).
28. Häkkinen, S. & Rhines, P. B. Decline of subpolar North Atlantic circulation during the 1990s. *Science (80-)* **304**, 555 (2004).
29. Frankcombe, L. M. & Dijkstra, H. A. Coherent multidecadal variability in North Atlantic sea level. *Geophys. Res. Lett.* **36**, (2009).
30. Diabaté, S. T. et al. Western boundary circulation and coastal sea-level variability in Northern Hemisphere oceans. *Ocean Sci.* **17**, 1449–1471 (2021).
31. Kenigson, J. S., Han, W., Rajagopalan, B., Yanto & Jasinski, M. Decadal shift of NAO-linked interannual sea level variability along the U.S. northeast coast. *J. Clim.* **31**, 4981–4989 (2018).
32. Deser, C. & Blackmon, M. L. Surface climate variations over the North Atlantic Ocean during Winter: 1900–1989. *J. Clim.* **6**, 1743–1753 (1993).
33. Chang, P., Ji, L. & Li, H. A decadal climate variation in the tropical Atlantic Ocean from thermodynamic air–sea interactions. *Nature* **385**, 516–518 (1997).
34. Venegas, S. A., Mysak, L. A. & Straub, D. N. Atmosphere–Ocean coupled variability in the South Atlantic. *J. Clim.* **10**, 2904–2920 (1997).
35. Cane, M. A., Clement, A. C., Murphy, L. N. & Bellomo, K. Low-pass filtering, heat flux, and Atlantic multidecadal variability. *J. Clim.* **30**, 7529–7553 (2017).
36. Duchon, C. E. Lanczos filtering in one and two dimensions. *J. Appl. Meteorol.* **18**, 1016–1022 (1979).
37. Mehta, V. M. Variability of the tropical ocean surface temperatures at decadal–multidecadal timescales. Part I: The Atlantic Ocean. *J. Clim.* **11**, 2351–2375.
38. Nnamchi, H. C., Latif, M., Keenlyside, N. S., Kjellsson, J. & Richter, I. Diabatic heating governs the seasonality of the Atlantic Niño. *Nat. Commun.* **12**, 376 (2021).
39. Fasullo, J. T. & Gent, P. R. On the relationship between regional ocean heat content and sea surface height. *J. Clim.* **30**, 9195–9211 (2017).
40. Årthun, M., Wills, R. C. J., Johnson, H. L., Chafik, L. & Langehaug, H. R. Mechanisms of decadal North Atlantic climate variability and implications for the recent cold anomaly. *J. Clim.* **34**, 3421–3439 (2021).
41. Gulev, S. et al. North Atlantic Ocean control on surface heat flux on multidecadal timescales. *Nature* **499**, 464–467 (2013).
42. Yang, J. A linkage between decadal climate variations in the Labrador Sea and the tropical Atlantic Ocean. *Geophys. Res. Lett.* **26**, 1023–1026 (1999).
43. Johnson, H. L. & Marshall, D. P. Localization of abrupt change in the North Atlantic thermohaline circulation. *Geophys. Res. Lett.* **29**, 1–4 (2002).
44. Zhang, R. Latitudinal dependence of Atlantic meridional overturning circulation (AMOC) variations. *Geophys. Res. Lett.* **37**, 1–6 (2010).
45. Berglund, S., Döös, K., Groeskamp, S. & McDougall, T. J. The downward spiralling nature of the North Atlantic Subtropical Gyre. *Nat. Commun.* **13**, 1–9 (2022).
46. Farneti, R. & Vallis, G. K. Mechanisms of interdecadal climate variability and the role of ocean–atmosphere coupling. *Clim. Dyn.* **36**, 289–308 (2011).
47. Delworth, T. L. et al. The central role of ocean dynamics in connecting the North Atlantic oscillation to the extratropical component of the Atlantic multidecadal oscillation. *J. Clim.* **30**, 3789–3805 (2017).
48. Servain, J., Wainer, I., McCreary, J. P. & Dessier, A. Relationship between the equatorial and meridional modes of climatic variability in the Tropical Atlantic. *Geophys. Res. Lett.* **26**, 485–488 (1999).
49. Watanabe, M. & Kimoto, M. Tropical–extratropical connection in the Atlantic atmosphere–ocean variability. *Geophys. Res. Lett.* **26**, 2247–2250 (1999).
50. Smirnov, D. & Vimont, D. J. Extratropical forcing of tropical Atlantic variability during boreal summer and fall. *J. Clim.* **25**, 2056–2076 (2012).
51. Brayshaw, D. J., Hoskins, B. & Blackburn, M. The basic ingredients of the North Atlantic storm track. Part I: Land–Sea contrast and orography. *J. Atmos. Sci.* **66**, 2539–2558 (2009).
52. Omrani, N.-E., Keenlyside, N. S., Bader, J. & Manzini, E. Stratosphere key for wintertime atmospheric response to warm Atlantic decadal conditions. *Clim. Dyn.* **42**, 649–663 (2014).
53. Costa, E. D. D. & Verdiere, A. C. D. The 7–7-year North Atlantic Oscillation. *Q. J. R. Meteorol. Soc.* **128**, 797–817 (2002).
54. Gray, L. J., Woollings, T. J., Andrews, M. & Knight, J. Eleven-year solar cycle signal in the NAO and Atlantic/European blocking. *Q. J. R. Meteorol. Soc.* **142**, 1890–1903 (2016).
55. McCarthy, G. D., Joyce, T. M. & Josey, S. A. Gulf stream variability in the context of quasi-decadal and multidecadal Atlantic climate variability. *Geophys. Res. Lett.* **45**, 11,257–11,264 (2018).
56. Bryden, H. L., King, B. A., McCarthy, G. D. & McDonagh, E. L. Impact of a 30% reduction in Atlantic meridional overturning during 2009–2010. *Ocean Sci.* <https://doi.org/10.5194/os-10-683-2014> (2014).
57. Smith, D. M. et al. Robust skill of decadal climate predictions. *npj Clim. Atmos. Sci.* **2**, 1–10 (2019).
58. Smith, D. M. et al. North Atlantic climate far more predictable than models imply. *Nature* **583**, 796–800 (2020).
59. Rayner, N. A. et al. Global analyses of sea surface temperature, sea ice, and night marine air temperature since the late nineteenth century. *J. Geophys. Res. Atmos.* **108**, (2003).
60. de Boissésion, E., Balmaseda, M. A. & Mayer, M. Ocean heat content variability in an ensemble of twentieth century ocean reanalyses. *Clim. Dyn.* **50**, 3783–3798 (2018).
61. Poli, P. et al. ERA-20C: An atmospheric reanalysis of the twentieth century. *J. Clim.* **29**, 4083–4097 (2016).
62. Yanai, M., Esbensen, S. & Chu, J.-H. Determination of Bulk Properties of Tropical Cloud Clusters from Large-Scale Heat and Moisture Budgets. *J. Atmos. Sci.* **30**, 611–627 (1973).
63. North, G. R., Bell, T. L., Cahalan, R. F. & Moeng, F. J. Sampling errors in the estimation of empirical orthogonal functions. *Mon. Weather Rev.* **110**, 699–706.
64. Bretherton, C. S., Widmann, M., Dymnikov, V. P., Wallace, J. M. & Bladé, I. The Effective Number of Spatial Degrees of Freedom of a Time-Varying Field. *J. Clim.* **12**, 1990–2009 (1999).
65. Woodworth, P. L., Maqueda, M. Á. M., Roussenov, V. M., Williams, R. G. & Hughes, C. W. Mean sea-level variability along the northeast American Atlantic coast and the roles of the wind and the overturning circulation. *J. Geophys. Res. Ocean.* **119**, 8916–8935 (2014).
66. Piecuch, C. G. et al. How is New England Coastal Sea Level Related to the Atlantic Meridional Overturning Circulation at 26° N? *Geophys. Res. Lett.* **46**, 5351–5360 (2019).
67. Hayashi, Y. Space time cross spectral analysis using the maximum entropy method. *J. Meteorol. Soc. Jpn.* **59**, 621–624 (1981).
68. Daniell, P. J. Discussion of ‘On the theoretical specification and sampling properties of autocorrelated time-series’. *J. Royal Stat. Soc.* **8**, 88–90 (1946).
69. Årthun, M. et al. Skillful prediction of northern climate provided by the ocean. *Nat Commun* **8**, 15875 (2017).
70. Thompson, R. O. R. Y. Coherence Significance Levels. *J. Atmos. Sci.* **36**, 2020–2021 (1979).

Acknowledgements

H.C.N. was funded by the Deutsche Forschungs Gemeinschaft (DFG) grant 456490637, and was initially supported by the associateship scheme of the Abdus Salam International Centre for Theoretical Physics, Trieste, Italy. H.C.N. greatly acknowledges discussions on the roles of turbulent fluxes with Sergey Gulev. N.S.K. was funded by the European Union’s Horizon 2020 research and innovation programme (grant no. 817578, TRIATLAS) and the Research Council of Norway funded JPI Climate and JPI Ocean project (grant no. 317267, EUREC4OA).

Author contributions

The concept was devised and iterated on in discussions between H.C.N., R.F., N.S.K., F.K., M.L., A.R., and T.M. H.C.N. performed the analysis and plotted the figures. H.C.N. and M.L. led the writing of the manuscript. All authors contributed to interpreting the results, discussion of the mechanisms and improvement of this paper.

Funding

Open Access funding enabled and organized by Projekt DEAL.

Competing interests

The authors declare no competing interests.

Additional information

Supplementary information The online version contains supplementary material available at <https://doi.org/10.1038/s43247-023-00781-x>.

Correspondence and requests for materials should be addressed to Hyacinth C. Nnamchi.

Peer review information *Communications Earth & Environment* thanks the anonymous reviewers for their contribution to the peer review of this work. Primary Handling Editors: Heike Langenberg. Peer reviewer reports are available.

Reprints and permission information is available at <http://www.nature.com/reprints>

Publisher’s note Springer Nature remains neutral with regard to jurisdictional claims in published maps and institutional affiliations.



Open Access This article is licensed under a Creative Commons Attribution 4.0 International License, which permits use, sharing, adaptation, distribution and reproduction in any medium or format, as long as you give appropriate credit to the original author(s) and the source, provide a link to the Creative Commons license, and indicate if changes were made. The images or other third party material in this article are included in the article's Creative Commons license, unless indicated otherwise in a credit line to the material. If material is not included in the article's Creative Commons license and your intended use is not permitted by statutory regulation or exceeds the permitted use, you will need to obtain permission directly from the copyright holder. To view a copy of this license, visit <http://creativecommons.org/licenses/by/4.0/>.

© The Author(s) 2023